CB July 1942

NATIONAL ADVISORY COMMITTEE FOR AERONAUTICS

WARTIME REPORT

ORIGINALLY ISSUED
July 1942 as
Confidential Bulletin

PRELIMINARY EXPERIMENTAL INVESTIGATION OF AIRFOILS IN CASCADE

By Arthur Kantrowitz and Fred L. Daum

Langley Memorial Aeronautical Laboratory
Langley Field, Va.

NACA

WASHINGTON

L – 231

which the air is turned by the blades. A yaw survey with no blades in the tunnel and with straight walls showed that, in the region between the second and the fourth blades, the air angle was constant to within 1/2°.

It was found in these tests that the static pressure in the survey plane one-half chord behind the airfoils was always close to atmospheric pressure and this fact is used later to simplify the analysis.

SYMBOLS

α_1 angle between initial air and tangent to concave surface of blades

α_o angle between mean air and tangent to concave surface of blades

q local dynamic pressure

q_1 dynamic pressure of initial air

q_2 dynamic pressure of air one-half chord behind blades

q_o dynamic pressure of mean air

q_f final dynamic pressure of air after idealized mixing

p_1 static pressure measured by row of orifices ahead of blades

p_2 static pressure one-half chord behind the blades, equal to atmospheric pressure

Δp pressure rise across cascade $(p_2 - p_1)$

p_f final static pressure after idealized mixing

u_1 velocity of initial air

u_{ax} velocity in axial direction

u_2 velocity of air behind blades

u_{2_o} velocity of air outside wake in plane of A_2

u_o mean velocity

Δu vector difference of velocities $(u_1 - u_2)$

u_f final velocity of air after idealized mixing

S area of blade

s solidity, chord of blades divided by gap between them

C_{L_1} lift coefficient $(\text{lift}/q_1 s)$

$$C_{L_0} = \frac{\text{lift}}{q_0 s} = \frac{q_0}{q_1} C_{L_1}$$

A_1 cross-sectional area of initial air stream that passes between adjacent blades

A_2 area of air stream between adjacent blades one-half chord behind blades

θ angle through which air is turned by blades

ρ air density

ΔH total-head defect

β stagger

F force on blades

DATA AND ANALYSIS

Turning effectiveness of the blades.- The angle θ through which the air was turned by the blades is plotted in figure 3 against α_1, the angle between the initial air and the tangent to the concave surface of the blades. The angles given are averages taken over the air in the central vertical plane between the second and the fourth blades with the region in the blade wakes excluded. It will be noticed that $d\theta/d\alpha_1$ is close to unity, which illustrates that the behavior of the cascade with a solidity of unity is much closer to the infinite-solidity case $d\theta/d\alpha_1 = 1$ than to the isolated-airfoil case $d\theta/d\alpha = 0$.

Pressure distribution and lift.- It seems to be customary to base blade characteristics on "mean-air" conditions. A mean-velocity vector u_o (fig. 3) halfway between the initial air vector u_1 and the final air vector u_2 is used as the basis for determining q_o, α_o, and C_{L_o}. In figures 4 and 5 the pressure distributions obtained from orifices in the central airfoil are given. The quantity plotted is the difference between initial impact pressure q_1 and local static pressure divided by q_o, which is equal to the local dynamic pressure q divided by q_o. The values of atmospheric pressure p_2 and the static pressure ahead of the blades p_1 are also indicated on the graphs as differences in total head divided by q_o.

The values of lift coefficients C_{L_o} given in figures 4 and 5 were obtained from the pressure distributions by the use of a planimeter. They are plotted as circles in figures 6 and 7. In figure 7 the lift coefficients C_{L_1} and angles of attack α_1 are based on initial air conditions.

The force on the blades can also be computed from momentum considerations. There is a force parallel to the stagger line owing to the fact that the air has been turned, per blade

$$\rho u_{ax} \Delta u S/s \tag{1}$$

There is a force perpendicular to the stagger line owing to the pressure rise across the cascade, per blade

$$\Delta p S/s \tag{2}$$

The square of the force on the blades is then

$$F^2 = (\rho u_{ax} \Delta u S/s)^2 + (\Delta p S/s)^2 \tag{3}$$

If the drag forces are neglected, this force can be related to the lift coefficient C_{L_1} to give

$$C_{L_1}{}^2 = \frac{F^2}{\left(\frac{1}{2}\ \rho u_1{}^2 S\right)^2} = \left(\frac{2u_{ax}\Delta u}{u_1{}^2 s}\right)^2 + \left(\frac{\Delta p}{q_1 s}\right)^2 \tag{4}$$

From figure 3

$$\frac{u_{ax}}{u_1} = \cos \beta$$

$$\frac{\Delta u}{u_1} = \frac{u_{ax}}{u_1} [\tan \beta - \tan (\beta - \theta)]$$

Then

$$C_{L_1}{}^2 = \left[\frac{2 \cos^2 \beta \ [\tan \beta - \tan(\beta - \theta)]}{s}\right]^2 + \left(\frac{\Delta p}{q_1 s}\right)^2$$

or in the case covered by these tests $\beta = 45^\circ$ and $s = 1$, so that

$$C_{L_1}{}^2 = \left[1 - \tan (\beta - \theta)\right]^2 + \left(\frac{\Delta p}{q_1}\right)^2 \qquad (5)$$

The values of C_{L_1} and C_{L_0} obtained from equation (5) are plotted against α_1 and α_0, respectively, as crosses in figures 6 and 7. The agreement between the two methods of calculating may be taken as a measure of the accuracy of the present investigation. In figure 8, C_{L_0} is plotted against α_1 to serve as a correlation between the two methods of expressing the data.

Pressure rise across the cascade.- The pressure rises across the cascade - that is, the differences between the static pressure measured ahead of the blades and the atmospheric pressure - divided by the initial dynamic pressures are plotted as circles in figure 9. This plot can be compared with the pressure rise that would have been obtained if no energy losses had occurred. In the absence of energy losses, the pressure rise can be determined from figure 10. From the figure and the fact that the fluid may be considered incompressible

$$\frac{u_2}{u_1} = \frac{\cos \beta}{\cos (\beta - \theta)} = \sqrt{\frac{q_2}{q_1}} \qquad (6)$$

and from Bernoulli's theorem

$$p_2 - p_1 = q_1 - q_2 \tag{7}$$

$$\frac{\Delta p}{q_1} = 1 - \frac{q_2}{q_1} = 1 - \left[\frac{\cos \beta}{\cos (\beta - \theta)}\right]^2 \tag{8}$$

Points obtained from equation (8) and the measured values of θ are plotted as squares in figure 9. It can be seen from figure 9 or figure 1 that the blades continue to turn the air even after they are completely stalled. The pressure rise that might be expected to accompany the increase in the area of the stream produced by the turning, however, does not occur.

Losses in the cascade.- The difference between the curves of figure 9 indicated by circles and those indicated by squares must be attributed to energy losses in the flow through the cascade. In order to measure the part of this discrepancy that should be attributed to the drag of the blade, a rake of total-head tubes was used to survey the wake in the central vertical plane one-half chord length behind the central blade. A first approximation to the blade-drag losses can be found from a simple total-head integral. The energy defect (assuming constant static pressure) is

$$\text{Energy defect} = \int_{A_2} u_2 \Delta H dA_2 \tag{9}$$

where ΔH is the total-head defect in the element of area dA_2. If the total-head defect is not very large anywhere in the wake $u_2 \cong \overline{u}_2$ (the average of u_2 over A_2) and the energy defect may be written

$$\text{Energy defect} = \overline{u}_2 \int_{A_2} \Delta H dA_2 \tag{10}$$

Equation (10) was made nondimensional by dividing by the total kinetic energy entering the cascade to obtain

$$\frac{\text{energy defect}}{\text{initial kinetic energy}} = \frac{\overline{u}_2 \int_{A_2} \Delta H dA_2}{q_1 u_1 A_1} = \frac{\int_{A_2} \Delta H dA_2}{q_1 A_2} \tag{11}$$

This quantity is plotted in figure 11.

The pressure rise across the cascade will now be corrected for these measured blade-drag losses. Since the static pressure was nearly constant everywhere,

$$\Delta H = \frac{1}{2} \rho u_{2_0}{}^2 - \frac{1}{2} \rho u_2{}^2$$

or

$$u_2 = \sqrt{u_{2_0}{}^2 - \frac{\Delta H}{\frac{1}{2} \rho}}$$

and from continuity

$$u_1 A_1 = \int_{A_2} u_2 dA_2 = \int_{A_2} \sqrt{u_{2_0}{}^2 - \frac{\Delta H}{\frac{1}{2} \rho}} \, dA_2$$

hence

$$1 = \frac{A_2}{A_1} \int_{A_2} \sqrt{\frac{u_{2_0}{}^2}{u_1{}^2} - \frac{\Delta H}{q_1}} \frac{dA_2}{A_2}$$

Now since u_{2_0} is the velocity outside the wake

$$\frac{1}{2} \rho u_1{}^2 + p_1 = \frac{1}{2} \rho u_{2_0}{}^2 + p_2$$

and

$$\frac{\Delta p}{q_1} = 1 - \frac{u_{2_0}{}^2}{u_1{}^2}$$

hence

$$1 = \frac{A_2}{A_1} \int_{A_2} \sqrt{\frac{\Delta p}{q_1} - \frac{\Delta H}{q_1}} \frac{dA_2}{A_2} \qquad (12)$$

The pressure rise across the cascade can be determined from equation (12) by a trial-and-error procedure if the total-head losses are known. In cases where $\Delta H/q_1$ is always small compared with $1 - \frac{\Delta p}{q_1}$, the square root in equation (12) can be expanded by the binomial theorem and reduced to a form that is easier to solve for Δp. If only the first two terms in the expansion are retained, equation (12) becomes

$$\left(1 - \frac{\Delta p}{q_1}\right)\frac{A_2}{A_1} - \sqrt{1 - \frac{\Delta p}{q_1}} - \frac{1}{2}\frac{A_2}{A_1}\int_{A_2} \frac{\Delta H}{q_1}\frac{dA_2}{A_2} = 0 \qquad (13)$$

The pressure rise across the cascade may then be found from equation (13) when $\Delta H/q_1$ is small. These pressure rises are calculated from equations (12) and (13) and are plotted as the middle curve in figure 9. Equation (13) was used for the low-drag region where the wakes were not very deep.

It will be seen that a large part of the differences between theory and experiment are not attributable to the drag of the blades in the central plane. It was therefore decided to survey the entire area A_2 (on one side of the central plane) at a single angle of attack, $\alpha_1 = 12^\circ$, to determine the cause of the remaining discrepancy. The results of the total-head survey are shown in figure 12. The figure is in the plane of A_2 one-half chord length behind the central airfoil. The lines in the figure are contours of equal total-head defect and the numbers on the contours are the percentages of initial total head lost. The losses along the walls are seen to be very important.

The pressure rise across the cascade was then determined by evaluating the integral in equation (12) from the general survey shown in figure 12. The value obtained was $\frac{\Delta p}{q_1} = 0.281$. The agreement between this value and the experimental point 0.271 is now within experimental error.

If the air leaving the cascade were allowed to mix without net loss of momentum, a greater pressure rise would be obtained (mentioned later). The measured pressure rise will depend, in general, upon the distance that has been allowed for the wake to mix with the surrounding air. In order to obtain a comparison with the perfect-fluid pressure rise that would be independent of the arbitrary choice of the survey plane A_2, the pressure rise due to idealized mixing will now be added to p_2.

Consider that the stream leaving the cascade is allowed to mix with the total momentum and with the cross-sectional area A_2 unchanged. The final velocity u_f and the final pressure p_f can then be found from continuity

$$u_1A_1 = \int_{A_2} u_2 dA_2 = u_f A_2 \qquad (14)$$

and conservation of momentum

$$p_f A_2 + \rho_f u_f^2 A_2 = \int_{A_2} \rho u_2^2 dA_2 + A_2 p_2$$

Since $\int_{A_2} \rho u_2^2 dA_2$ is always larger than $\rho u_f^2 A_2$, there will always be a pressure rise accompanying the mixing process. This pressure rise is

$$\frac{p_f - p_2}{q_1} = \frac{2}{A_2}\int \frac{q_2}{q_1} dA_2 - 2\frac{q_f}{q_1} \qquad (15)$$

The integral in equation (15) was obtained by finding the areas under the various contours of figure 12 with a planimiter. The value of q_f/q_1 was obtained from equation (14), the first and the second terms yielding 0.656 and 0.662, respectively. The inaccuracy of the measurements is indicated by this discrepancy. By use of q_f/q_1 = 0.659, it was found that $\frac{p_f - p_2}{q_1}$ = 0.020. Adding this value to the experimental value of $\Delta p/q_1$ gives $\frac{p_f - p_1}{q_1}$ = 0.291. This value is plotted as a plus sign in figure 9. Adding the idealized mixing pressure rise to the value of $\Delta p/q_1$ obtained theoretically by taking account of the complete exit survey gives 0.301. This value is plotted as a cross in figure 9. Comparison with the plus point shows a satisfactory agreement with the experimental results also corrected for idealized mixing.

The pressure rise found is thus freed from the arbitrary choice of the survey station. It is the maximum pressure rise that could be obtained by adding an idealized mixing channel after the cascade.

APPLICATION AND FUTURE PROGRAM

Two of the results of this work would appear general enough to be useful while further cascade work is in progress.

It will be noticed from figure 2 that $d\theta/d\alpha_1$ is close to unity; that is, close to the value that would be expected for infinite solidity. It would seem, as a reasonable surmise, that this result would apply generally for solidities of the order of 1 or greater. A test of a single blade in the cascade set-up showed that the angle of zero lift is nearly unaffected by the presence of the other blades. This result might also be presumed to apply generally when the solidity and the camber of the cascade are not too large. It seems likely, therefore, that there is a solidity range near unity obeying a simple relation of the form

$$\theta = k\ (\alpha_1 - \alpha_{1_0})$$

where k is an empirical factor that is between 1.0 and 0.9 for the conditions of these tests and α_{1_0} is the angle of zero lift of the isolated airfoil. This equation can be used together with a relation of the form of equation (8) to approximate the pressure rise across a cascade in the absence of losses.

The general survey (fig. 12) made at $\alpha_1 = 12^\circ$ showed that a large part of the energy losses are due to poor flow near the walls. The wall boundary layer near the convex surface of the blade was greatly thickened, as might be expected, for two reasons: First, this air had to flow against nearly the same unfavorable pressure gradients as the air that passed over the blade, whereas the wall air started with a developed boundary layer; second, the low-pressure region near the blade probably accumulated air from the boundary layer of the adjacent wall. Similarly, the high-pressure region near the concave surface of the blade appeared to repel its boundary layer, producing a thin-wall boundary layer near this surface. It would be expected that these effects would increase with increasing lift coefficient.

The importance of wall losses makes it imperative that they be considered in the design of blowers for high efficiency. The lift coefficient for optimum efficiency is reduced below that of maximum blade lift-drag ratio, as can be seen by comparing figures 9 and 11. In the case covered by these tests a lift coefficient C_{L_0} near 0.4 or 0.5 would appear to be most efficient. Under these conditions for the cascade investigated, the air stream is turned through an angle θ between 10° and 13°. Wall losses must be considered to be even more serious in the use of more highly cambered blades, because the minimum blade drag occurs at higher lift coefficients.

It is to be expected that wall losses would be increased by the presence of end gaps and relative motion between the blades and the adjacent wall; these design conclusions must therefore be considered only tentative.

CONCLUSIONS

1. The angle through which the air is turned by a cascade of blades with a solidity of 1 and a small camber is nearly equal to the angle of attack (with respect to the entering air) of the blades minus the angle of attack for zero lift of the isolated airfoil.

2. A large part of the loss in a cascade may be associated with the flow along the channel walls and particularly with a region of slow air near the junctures of the convex side of the blades with the walls.

Langley Memorial Aeronautical Laboratory,
National Advisory Committee for Aeronautics,
Langley Field, Va.

REFERENCE

1. Jacobs, Eastman N., Abbott, Ira H., and Davidson, Milton: Preliminary Low-Drag-Airfoil and Flap Data from Tests at Large Reynolds Numbers and Low Turbulence. NACA A.C.R., March 1942.

TABLE I

NACA 65,2-810 AIRFOIL

COMBINED WITH $y = 0.0015x$

Upper surface		Lower surface	
x (percent c)	y (percent c)	x (percent c)	y (percent c)
0	0	0	0
.260	.913	.740	-.513
.486	1.130	1.014	-.570
.949	1.510	1.551	-.654
2.143	2.274	2.857	-.786
4.591	3.448	5.409	-.920
7.072	4.371	7.928	-.979
9.569	5.149	10.431	-1.013
14.589	6.415	15.411	-1.031
19.629	7.386	20.371	-1.018
24.681	8.139	25.319	-.979
29.740	8.705	30.260	-.929
34.804	9.098	35.196	-.858
39.870	9.339	40.130	-.771
44.936	9.409	45.064	-.649
50.000	9.282	50.000	-.458
55.058	8.950	54.942	-.190
60.107	8.434	59.893	.134
65.143	7.744	64.857	.496
70.164	6.922	69.836	.854
75.171	6.025	74.829	1.135
80.162	5.024	79.838	1.344
85.137	3.935	84.863	1.449
90.104	2.810	89.896	1.326
95.065	1.612	94.935	.916
100.048	.142	99.952	-.142
L. E. radius: 0.666 percent c			

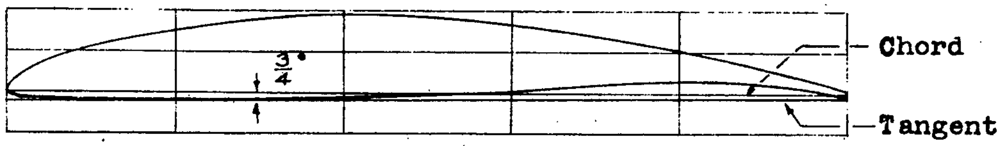

Blower-blade section NACA 65,2-810

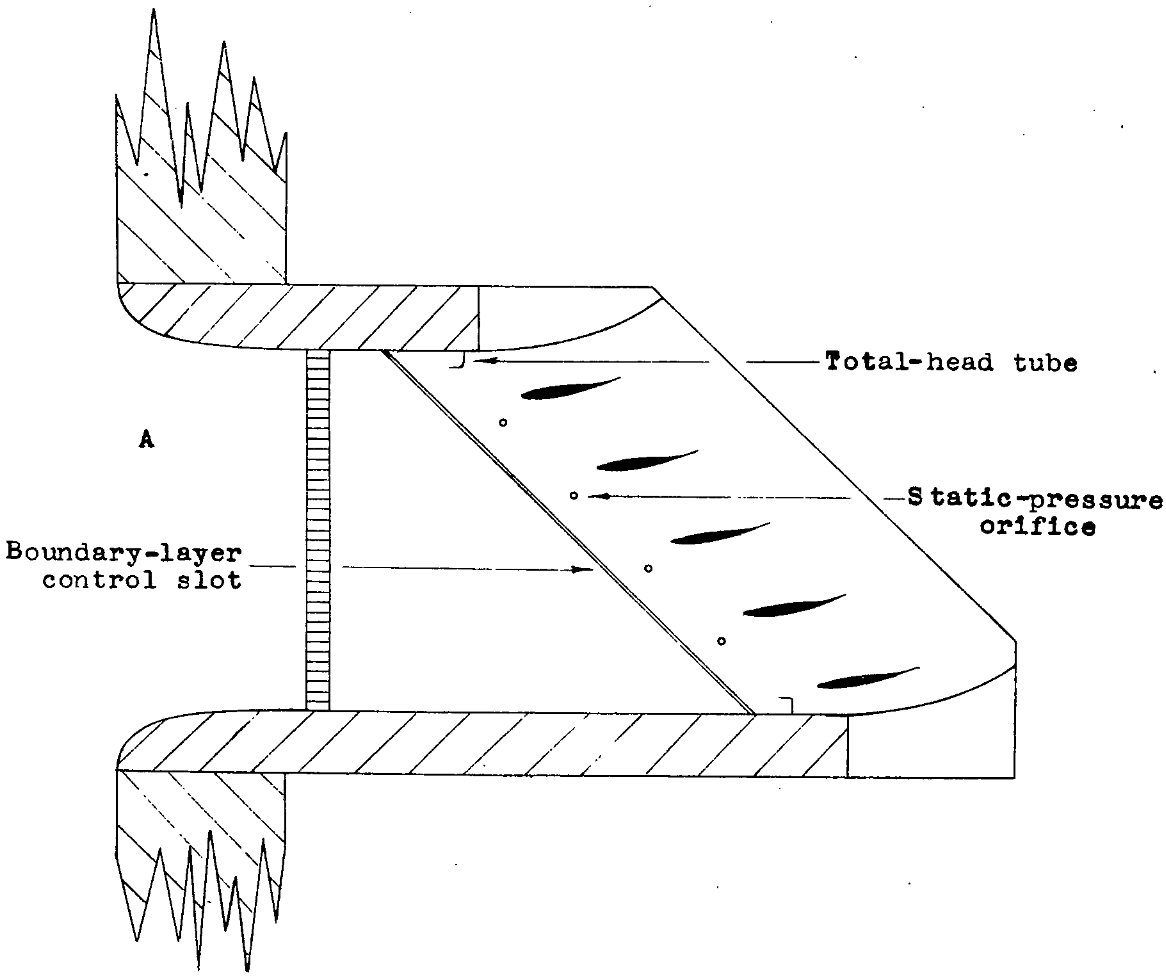

Figure 1.-Cascade testing apparatus.
Cascade of NACA 65,2-810 sections
Stagger: 45°; Solidity: 1

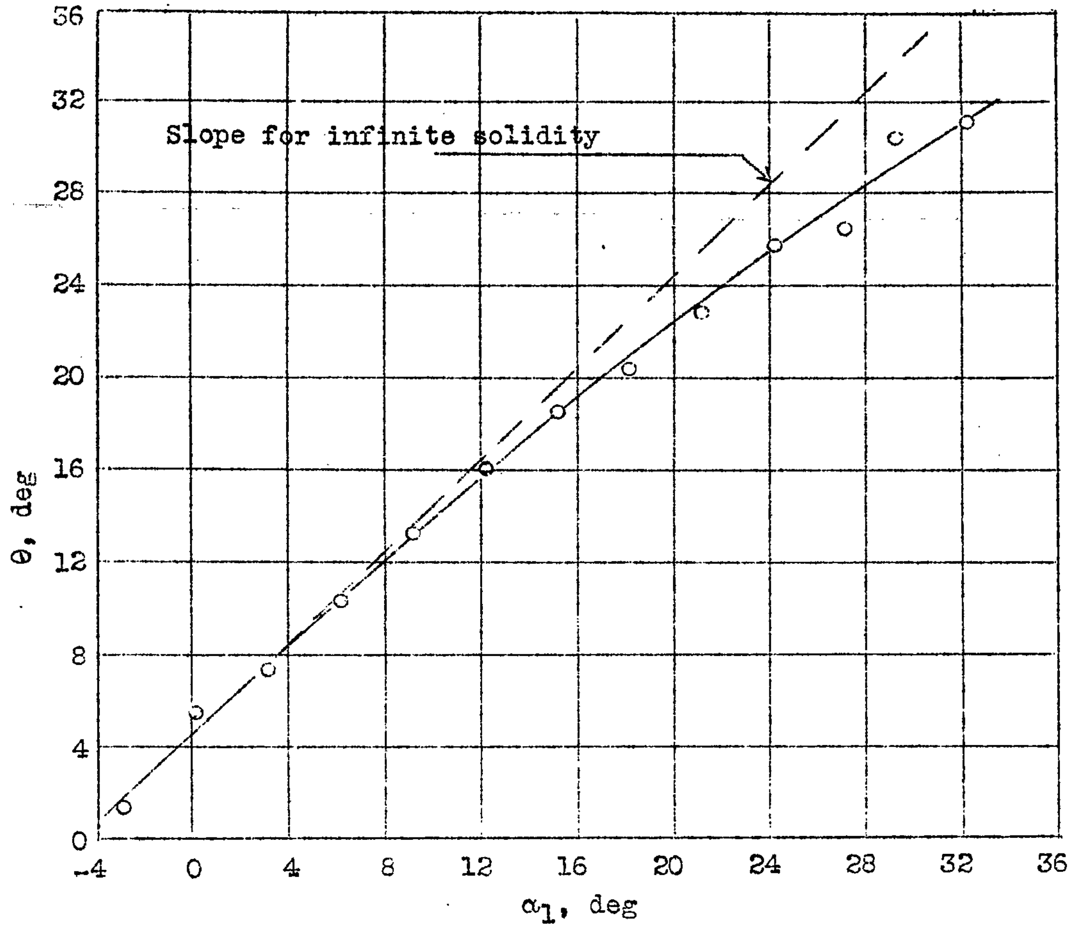

Figure 2.- Angle turned by air in passing through cascade. Cascade of NACA 65,2-810 sections; stagger: 45°; solidity: 1.

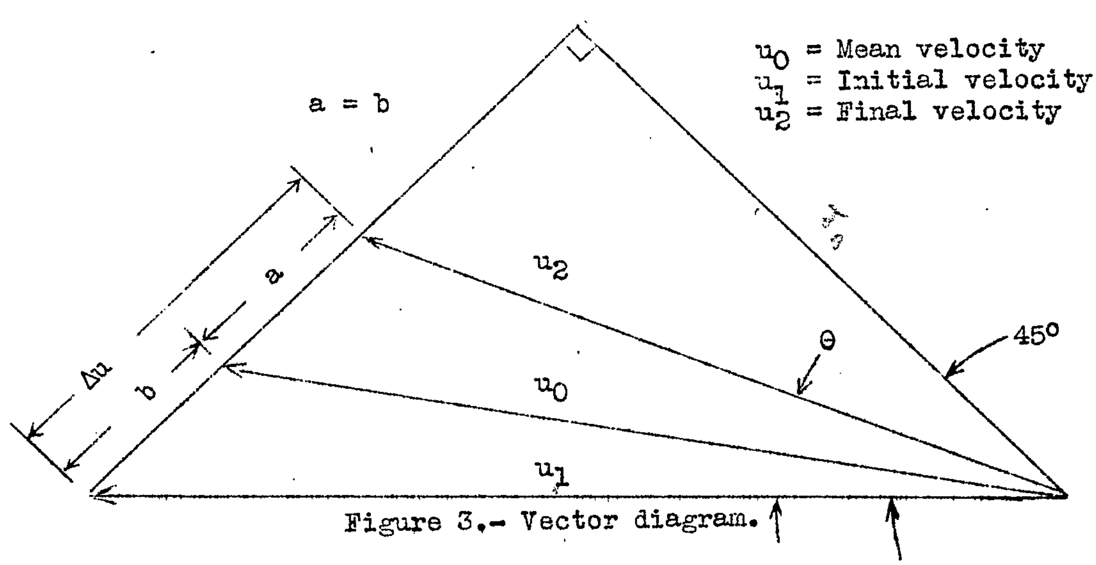

Figure 3.- Vector diagram.

Cascade of NACA 65,2-810 sections

Stagger 45°
Solidity: 1
Blade angles are measured relative to tangent to airfoil concave surface

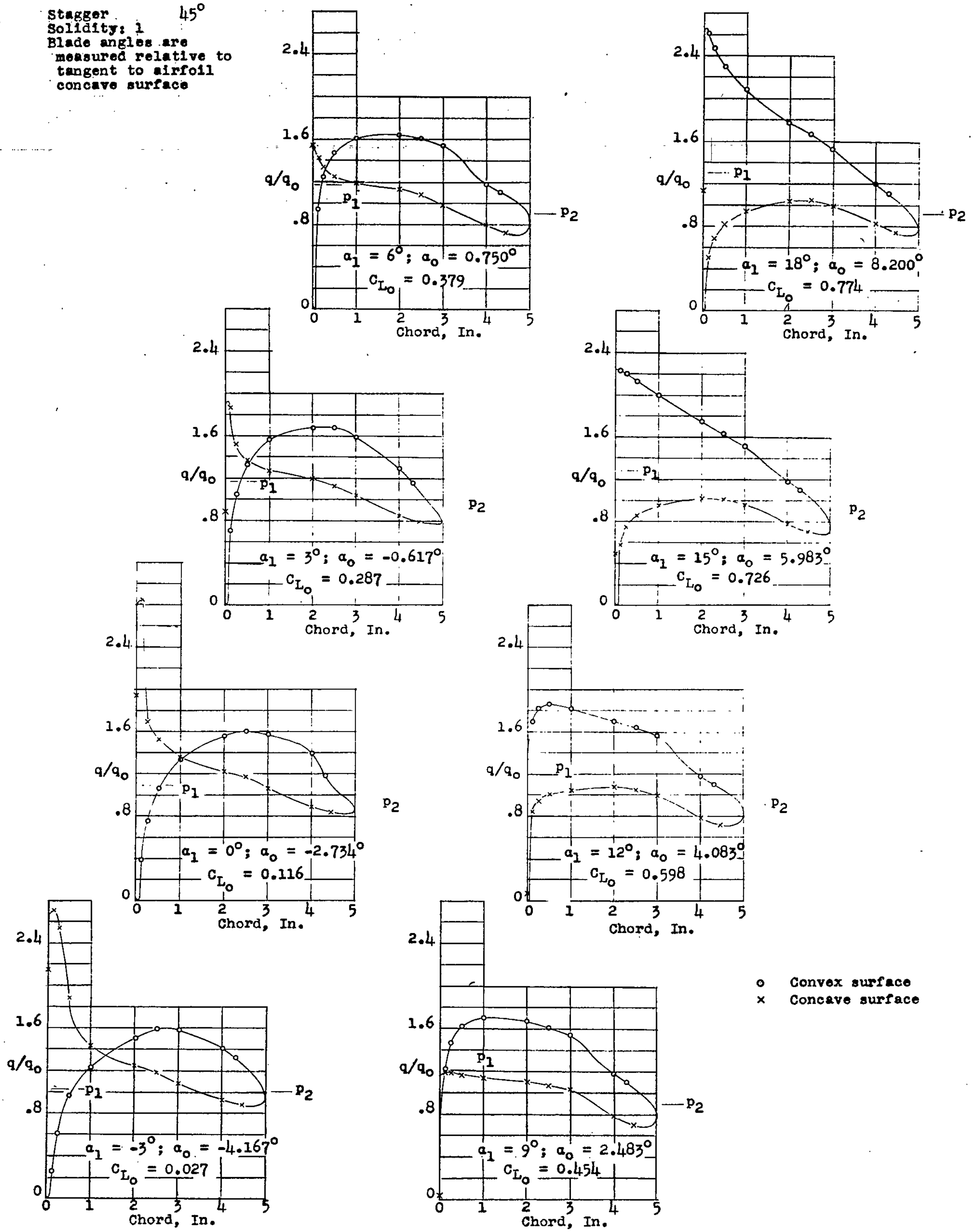

Figure 4.- Section pressure distributions.

L-231

Cascade of NACA 65,2-810 sections

Stagger 45°
Solidity: 1
Blade angles are measured relative to tangent to airfoil concave surface

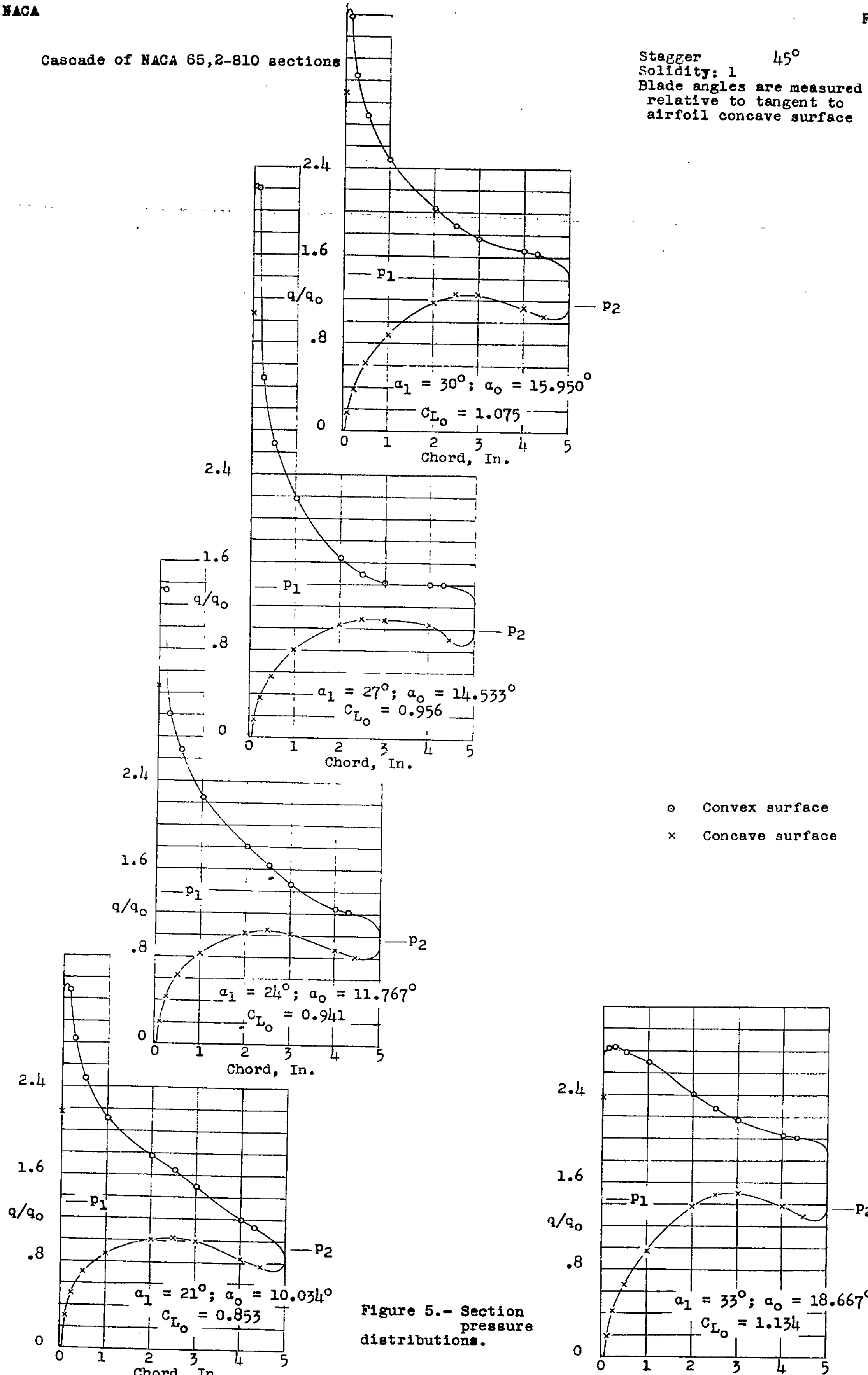

Figure 5.- Section pressure distributions.

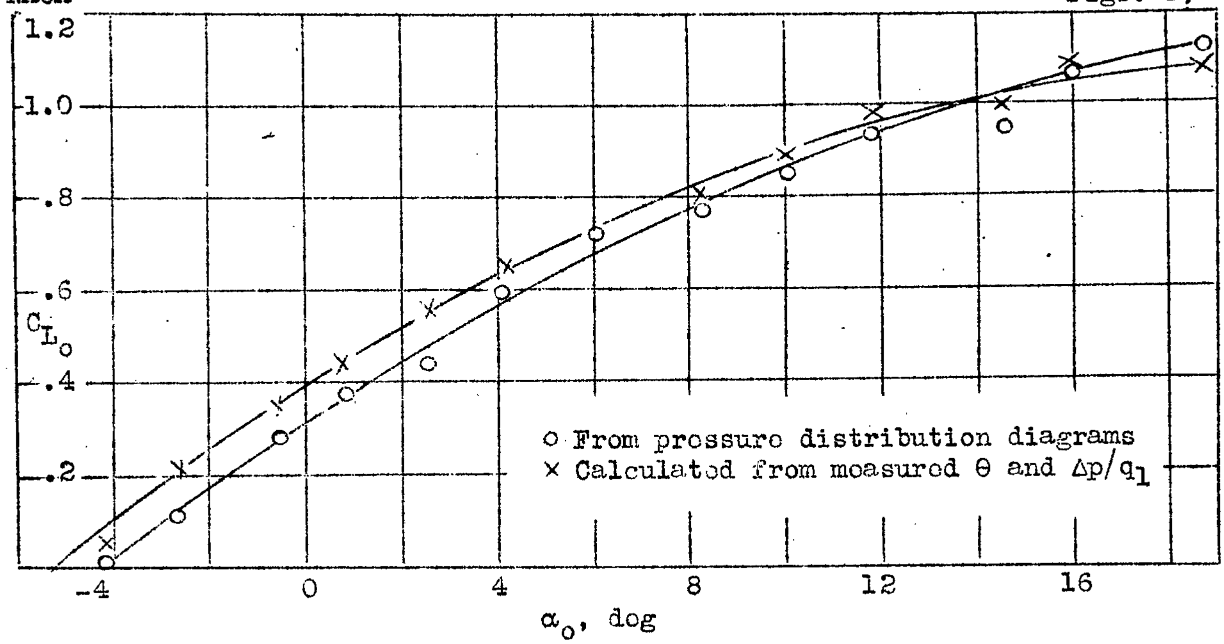

Figure 6.- Lift coefficients based on mean air conditions.
Cascade of NACA 65,2-810 sections;
Stagger: 45°; Solidity: 1.

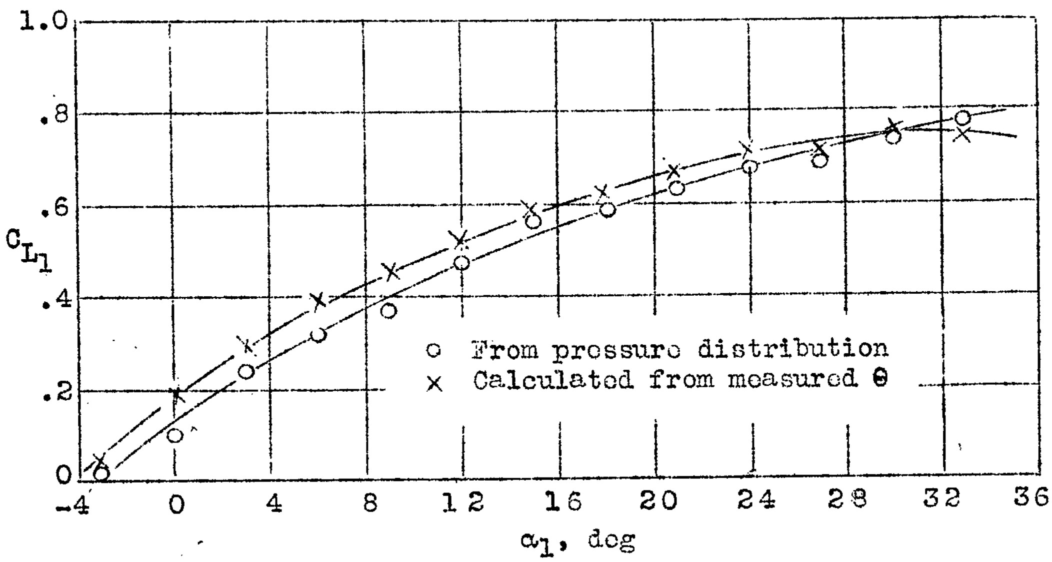

Figure 7.- Lift coefficents based on initial air conditions.
Cascade of NACA 65,2-810 sections;
Stagger: 45°; Solidity: 1.

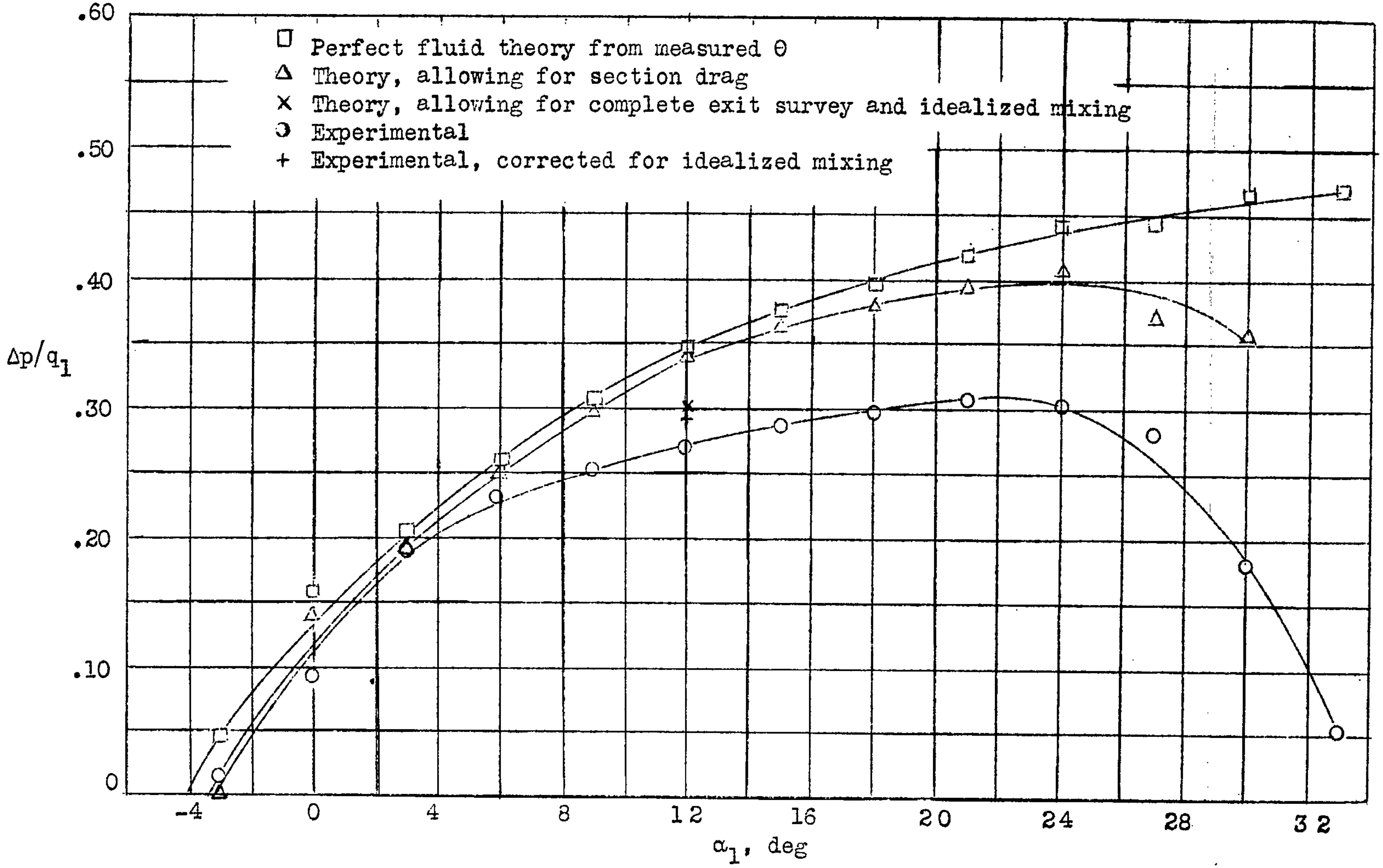

Figure 9.- Pressure rise across cascade. Cascade of NACA 65,2-810 sections; stagger, 45°; solidity, 1.

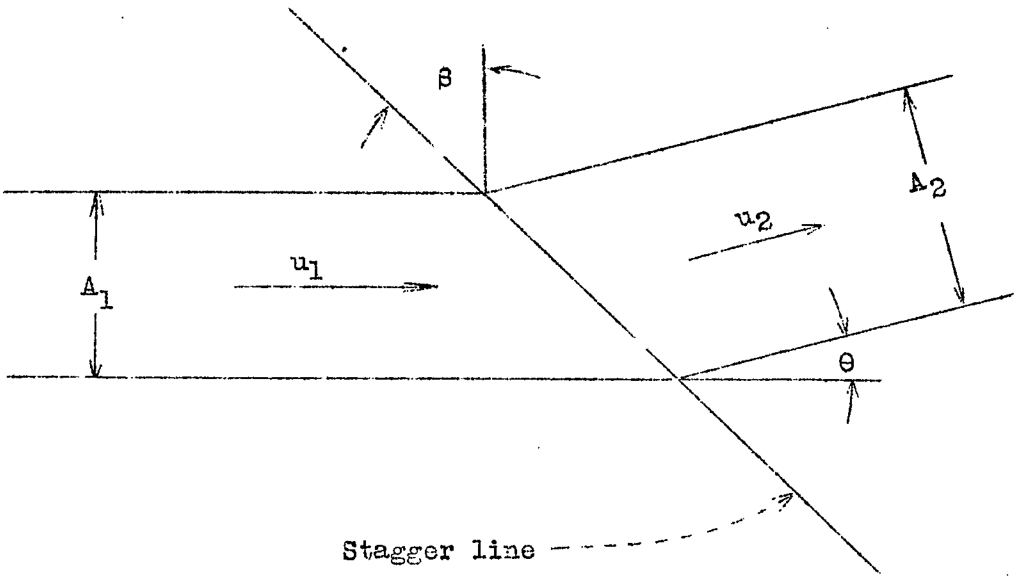

Figure 10.- Illustration for pressure-rise calculation. Cascade of NACA 65,2-810 sections; stagger, 45°; solidity, 1.

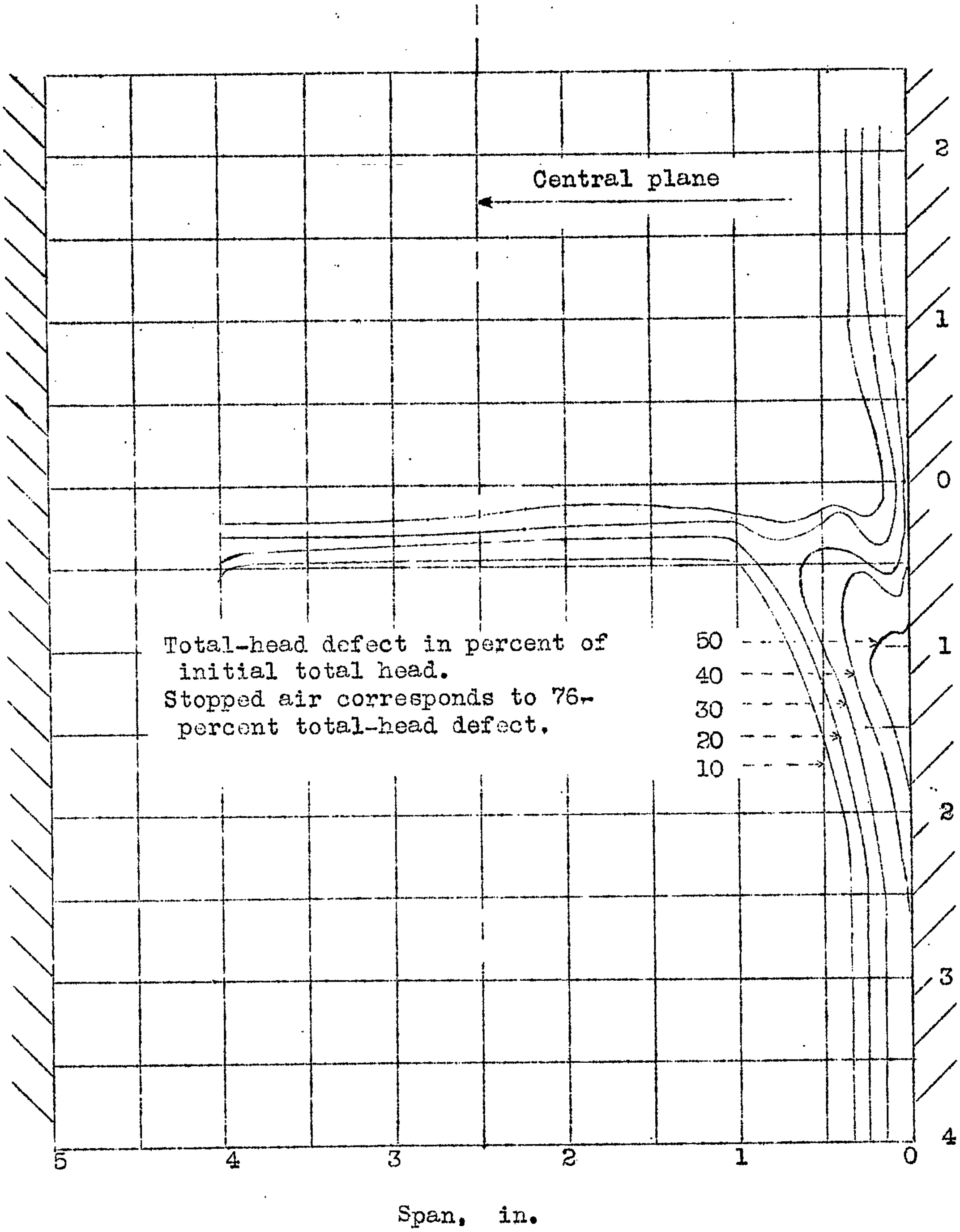

Figure 12.- Contours of constant total-head defect downstream of cascade. Cascade of NACA 65,2-810 sections; Stagger: 45°; α_1: 12°; Solidity: 1.